Published in Surface Science 331-333, issue 2, 1002-1014, 1995
which should be used for any reference to this work

Angle-scanned photoelectron diffraction

J. Osterwalder [a,*], P. Aebi [a], R. Fasel [a], D. Naumovic [a], P. Schwaller [a], T. Kreutz [a], L. Schlapbach [a], T. Abukawa [b], S. Kono [b]

[a] *Institut de Physique, Université de Fribourg, CH-1700 Fribourg, Switzerland*
[b] *R.I.S.M., Tohoku University, Sendai 980, Japan*

Abstract

A brief survey is given on the current state-of-the-art of this surface structural technique based on photoelectron spectroscopy, with particular emphasis on the progress that has been made recently by routinely measuring full-hemispherical intensity distributions. We limit the discussion to the photoelectron forward focusing regime, which is attained at electron kinetic energies of a few hundred eV. Surface bond directions are directly revealed as pronounced maxima in the angular distributions from subsurface atoms, while characteristic interference features are observed for surface species. For both cases the dependence on the atomic type is weak enough so that these features provide a fingerprint of the local bonding geometry. For surface and near-surface species, this may then serve as a starting point for a structure refinement using single-scattering cluster calculations. Selected examples are given for illustrating these procedures.

Keywords: Photoelectron diffraction; Surface structure

1. Introduction

Over the last few years photoelectron diffraction has evolved from an exotic phenomenon in angle-resolved X-ray photoelectron spectroscopy (XPS) to a widely accepted technique for obtaining detailed information on surface structure. The principles of the two closely related X-ray photoelectron diffraction (XPD) and Auger electron diffraction (AED), and their wide range of current and potential applications have been extensively described in various recent reviews [1–8]. In this paper we would like to highlight the particular progress that has been achieved recently in the routine measurement of complete two-dimensional (2D) angular distributions (2π-scans) of photoelectrons and Auger electrons, and how this availability of large data sets has facilitated the direct interpretation in terms of surface structure. This progress was to some extent motivated by the intriguing idea that such diffraction patterns could be viewed as photoelectron holograms [9] that could be reconstructed into real-space atomic images by a 2D phased Fourier transform [10]. This interesting direct method appears to work in several cases, but artifacts are usually present and the accuracy in the structural parameters is found to be only of the order of a few tenths of an ångström [5,6,8–13]. The main benefit lies in the provision of a useful starting point for the

* Corresponding author. New address: Physik-Institut, Universität Zürich-Irchel, Winterthurerstrasse 190, CH-8057 Zürich, Switzerland. E-mail: osterwal@uzph3.physik.unizh.ch; Fax: +41 1 257 5704.

structure refinement by model calculations, thus minimizing the cumbersome trial-and-error process. Our conclusion from the consideration of many experimental 2π-scans is that the emission pattern from a specific site above, within or below the surface is characteristic enough to provide a fingerprint for this site, permitting a first guess on the local geometry which is of similar quality as that from the holographic approach.

We shall discuss mainly the typical high-energy regime of XPD and AED, considering electron kinetic energies of at least a few hundred electronvolts. For this situation it has been recognized quite early that the strong peaking of the electron–atom scattering factor for small scattering angles, and the small scattering phase shift, produce electron emission patterns that are dominated by strong maxima along directions connecting the photoemitters with near-neighbour scattering atoms [14,15], as is illustrated in Fig. 1. This concentration of flux along internuclear axes is well understood theoretically [16] and has also been termed "forward focusing". To first approximation an emission pattern represents thus a forward-projected image of the crystal planes above the photoemitter, slightly modified by higher-order, energy-dependent interference structures and due to a different weighting of scatterers at different distances [17]. Consequently, subsurface emitters give a particularly clear fingerprint of their local bonding geometry, and we shall give a few illustrative examples in Section 4.

For surface species we start to realize that, while forward focusing maxima are present only parallel to the surface, the associated rise in intensity can still be observed in grazing emission and be used for a clear site determination. Furthermore, due to the absence of forward focusing signals for non-grazing angles, the higher-order interference structures are here well exposed. In Section 5 we shall present a few examples showing that these patterns show features characteristic for a specific bonding site, which are not too strongly dependent on the atomic types constituting the adsorbate system. Beforehand, some general remarks are given on experimental aspects related to measuring 2π-scans, and on a few theoretical aspects related to structure refinement by model calculations, an example of which is also given in Section 5.

2. Experimental aspects

For the measurement of 2π-scans of photoelectrons or Auger electrons various procedures have been adopted. The most simple one makes use of an angle-resolving electron energy analyzer, usually of hemispherical type, and scans the two emission angles θ and ϕ, corresponding to polar and azimuthal rotations, either by a rotation of the sample [17–21] or by moving the analyzer relative to the sample [22]. Data acquisition is thus sequential, and at each angular setting the full spectral information can readily be obtained, which is a requirement if, e.g., chemically-shifted states with considerable overlap within a spectrum are to be recorded separately. Alternatively, sophisticated electron-optical devices

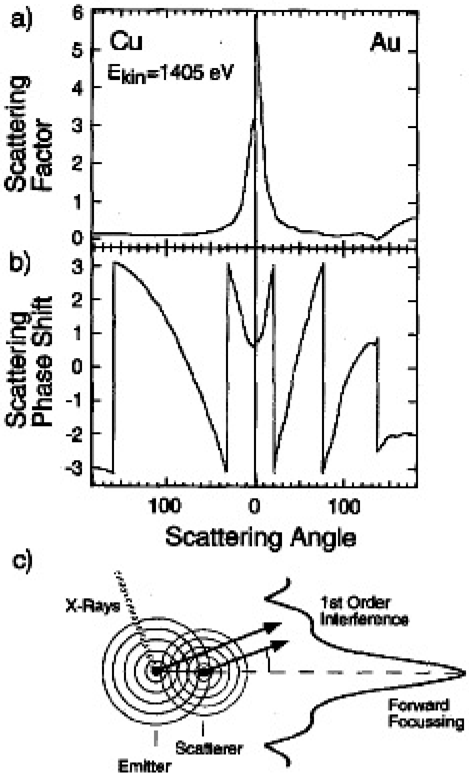

Fig. 1. (a) Atomic scattering factors calculated for Cu and Au scatterers for an incoming plane wave. A Cu_3Au muffin-tin potential has been used. (b) Plane wave scattering phase shifts for the same cases. (c) Illustration of the dominant elastic scattering processes associated with XPD, showing the axial symmetry of the diffraction pattern associated with an isolated scatterer.

have been designed to record either a full polar angle range [23,24], a part of an azimuthal angle range [25], or a large two-dimensional solid angle range [26,27] simultaneously. These devices bring a considerable reduction in data acquisition time which is crucial when studying reactive surfaces. Moreover, fixed crystal geometries are advantageous for experiments requiring a wide temperature range and precise temperature control. On the negative side, some of these devices suffer from detector inhomogeneities, low signal-to-background ratios, and marked energy-dependent angular distortions. Nevertheless, they have been successfully applied for measuring wide-angle substrate [28], thin film [29] and adsorbate [13] photoelectron diffraction patterns.

The combination of crystal rotation and a fixed hemispherical analyzer is the most widely used, mainly thanks to its flexibility and high degree of accuracy, and due to the fact that highly optimized analyzer designs are commercially available. Recent progress in detection sensitivity, data acquisition systems and data reduction has made it possible to sequentially collect photoelectron intensities at 4000 to 6000 angular settings, uniformly distributed over 2π solid angle [20,21]. We have adopted an azimuthal scanning mode, starting the measurements at grazing emission and reducing the polar angle after each full 360° rotation of the crystal. The advantage of this mode is that the symmetry of the pattern usually gives a reliable indication for the consistency of the data. Probing the grazing angles first minimizes the effects of sample contamination. Typical measuring times highly depend on the intensity of the photoemission signal of interest. They range from less than one hour for strong substrate signals and modest angular resolution (2–3° full cone) up to 24 h for submonolayer adsorbate emission. A careful verification of possible effects due to sample degradation is therefore mandatory, and in some cases several quicker measurements have to be summed to provide sufficient statistical accuracy. Progress is here possible with the latest designs of commercial spectrometers and excitation sources.

3. Theoretical considerations

A theoretical description of XPD and AED involves: (i) the excitation process producing a source electron wave with a given angular momentum symmetry centered at the emitting atom, (ii) the single and multiple elastic scattering of this wave off the atoms surrounding the emitter, (iii) inelastic scattering processes reducing the wave amplitude during its propagation to the surface, (iv) thermal vibrations reducing the weight of coherent elastic processes in a Debye–Waller type fashion, and (v) wave refraction at the surface potential step [1,5]. Theoretical modelling for XPD is in an advanced state much like that for low-energy electron diffraction (LEED), using either full multiple-scattering (MS) cluster-type approaches [1,5,30–32] or LEED-type layer-by-layer methods [33], and quantitative agreement is possible. There is, however, an ongoing discussion as to whether the much more efficient single scattering approximation can be reliably used for extensive structure searches. Clear cases have been identified where single-scattering-cluster (SSC) calculations show significant deficiencies as compared to MS calculations, as e.g. the reduction and narrowing of forward focusing maxima along chains of atoms [30,34–36]. Our experience is that, if such geometries can be avoided, meaningful structure searches can be carried out very efficiently using SSC calculations.

In the case of AED there is a further complication. The Auger process mixes many angular momentum final states, the weights of which are often not known, and which influence the diffraction patterns strongly in the low energy regime [37–39]. However, simple s-wave emission has proven adequate to some extent for modelling high-energy AED [4,6].

4. Subsurface species

4.1. *Substrate emission*

Much of the early experiments have been devoted to measuring substrate diffraction patterns in order to have well defined and well known crystal structures. The focus was on the physics of the scattering processes involved. In Fig. 2 we show experimental diffraction patterns of Cu 3p emission measured at 1178 eV kinetic energy from three different low-index surfaces of copper [17,40]. All patterns are dom-

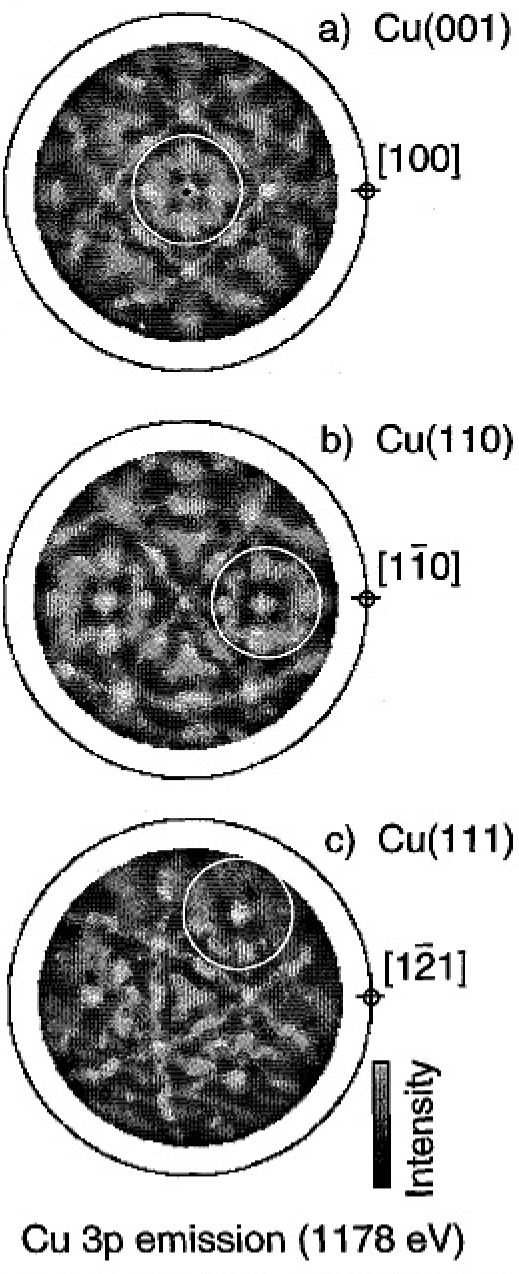

Fig. 2. Cu 3p emission patterns measured from three different low-index surfaces of copper (Refs. [17,40]). The Cu 3p intensity has been transformed into a linear grey scale while angles are projected stereographically: The center of each plot represents normal emission, the black circle indicates emission parallel to the surface. White circles mark characteristic interference patterns centered at ⟨100⟩ crystal directions.

inated by bright lines, representing enhanced emission along high-density crystal planes, and by bright maxima at crossings of such lines, which correspond to near-neighbour internuclear directions. Comparing the three different faces, Cu(001), Cu(110) and Cu(111), it is evident that each pattern is directly related to the others by a simple crystal rotation. In Fig. 2 the white circles mark a characteristic flower-like pattern centered on ⟨100⟩ directions. This feature is very similar for all three faces except for a slight distortion due to the stereographic projection. The patterns are thus determined rather by the three-dimensional bulk crystal structure than by the 2D surface termination, and information on the surface layers may be expected only at very grazing angles.

It has recently been demonstrated how a data base of such substrate patterns can be used in a fingerprint-type way for determining the internal structure of a growing thin film [41–43]. As an example we give in Fig. 3a the measured diffraction pattern of Ag 3d from a 84 Å thick film of Ag on a $Bi_2Sr_2CaCu_2O_8(001)$ surface [43]. In this case there was no indication of epitaxial growth from LEED measurements and scanning tunnelling microscopy (STM) data showed island formation without resolving the internal structure on the Ag islands [44]. In Fig. 3b the pattern of Pt 4f emission from a Pt(110) surface is given [21]. There is a correspondence of polar emission angles of two dominant maxima, which appear at $\theta = 62°$ in both patterns of Figs. 3a and 3b. Fig. 3c shows a superposition of the Pt(110) pattern with its replica after an azimuthal rotation of 109°, representing emission from two rotated domains. There is perfect agreement with Fig. 3a in all details, indicating growth of two domains of Ag(110) on this oxide surface as indicated in Fig. 3d. This type of fingerprint analysis is particularly useful in cases where the occurrence of domains makes an intuitive interpretation of the data difficult or when there is no complementary information from other techniques to provide a first guess on the structure.

4.2. Epitaxial growth and interface mixing

Maybe one of the most powerful and direct applications of XPD and AED is that of monitoring the growth of epitaxial thin films [2,4]. It is easily appreciated that if a thin film is deposited on a substrate and emission from the film is considered, each new layer produces a set of additional forward focusing maxima which represent thus a very clear signature for the local film thickness. It is in this respect important to emphasize the locality of this probe: If forward focusing maxima indicative of third-layer emission are observed this does not mean that two compact layers have formed and a third is building up. Rather it means that film atoms are present at positions that are covered by two further layers of material. An independent measure of the absolute coverage on the surface is needed which can to some extent be obtained by evaluating XPS film-to-substrate intensity ratios. Even if the absolute coverage is precisely known ambiguities concerning the interpretation of diffraction patterns in terms of a particular growth mode may remain: The formation of three-dimensional islands may produce local third-layer emitters, which on the other hand may also be produced by penetration of film atoms into the third substrate layer. It often takes further input from other experimental techniques to obtain the full picture.

The particular strength of XPD/AED in this sort of problem is its extreme sensitivity to buried emitters. Emitters within the top surface layer exhibit no forward focusing signals at non-grazing angles, usually showing anisotropies, defined as I_{max} −

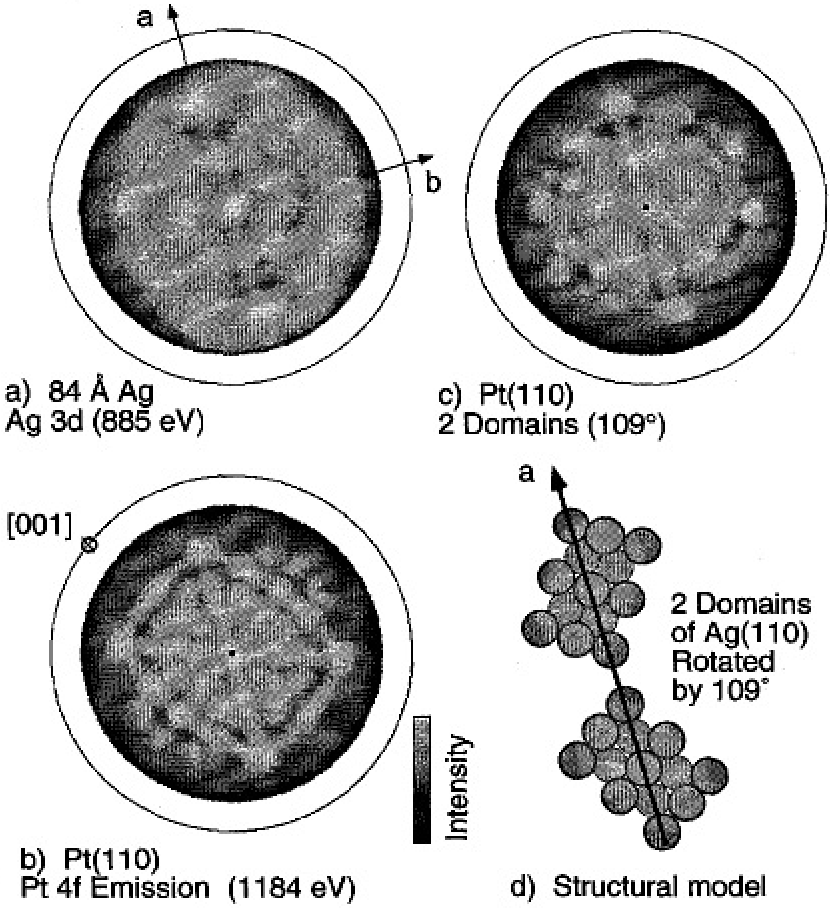

Fig. 3. (a) Ag 3d emission pattern from a 84 Å thick film of Ag on a cleaved $Bi_2Sr_2CaCu_2O_8(001)$ high-temperature superconductor surface (Ref. [43]). The directions *a* and *b* represent inequivalent main axes of this orthorhombic structure. (b) Pt 4f emission pattern from Pt(110) (Ref. [21]). (c) Superposition of the Pt 4f pattern of (b) with its own replica after an azimuthal rotation of 109°. (c) Illustration of the oriented two-domain structure of Ag islands.

I_{min}/I_{max}, of a few percent due to wave interference in this angular range. A second-layer emitter theoretically produces anisotropies of the order of 75%. From these numbers on finds that the coexistence of 1% of film atoms in second-layer positions and one completed surface layer leads to a forward focusing enhancement of about 2% which is measurable.

As an example for this type of morphological problem in thin film epitaxy we give in Fig. 4 Au 4d emission patterns for the beginning growth of Au on Cu(001) at three different coverages of 0.2, 0.4 and 0.6 monolayers (ML) [45]. The most striking feature is the appearance of distinct forward focusing maxima along ⟨110⟩ nearest neighbour (NN) and the [001] next-nearest neighbour (NNN) directions already at 0.6 ML, indicating the presence of a fair number of second and third layer emitters at this nominally submonolayer coverage. In order to unravel the morphology of this submonolayer system results from other techniques were needed. A quantitative LEED analysis of the $c(2 \times 2)$ structure seen in the half monolayer regime clearly revealed the formation of an ordered 2D Au/Cu alloy in the top layer [46], and a more recent STM study of the same system showed that alloy terraces nucleate and grow laterally as the coverage is increased [47]. The appearance of subsurface Au atoms is easily explained by this tendency of alloy formation: in order to enter the surface layer to form the alloy, Au atoms need to replace existing Cu atoms. These local exchange processes lead to a population of Cu atoms on top of the surface which can form new Au/Cu alloy terraces when more Au is added. What we learn from these XPD experiments is that, at room temperature, the interlayer exchange processes are frozen once a new terrace has grown over an existing one, keeping thus measurable numbers of second layer, and later third layer Au atoms inside the surface. A quantitative analysis of the Au 4d ⟨110⟩ forward focusing enhancement, which is 13% at 0.4 ML and 25% at 0.6 ML, yields second-layer Au populations of 3% and 9%, respectively.

In Section 5 it will be shown that measuring the Au 4d diffraction pattern at very low coverage and down to very grazing angles, the 2D alloy formation can also be seen directly from such data, and that the surface bond distance can be determined with equal accuracy as with LEED.

4.3. Reacted surfaces

Maybe one of the clearest examples for how XPD can monitor structural changes occurring due to a surface reaction is the investigation by Abukawa et al. [48] of the negative electron affinity (NEA) sur-

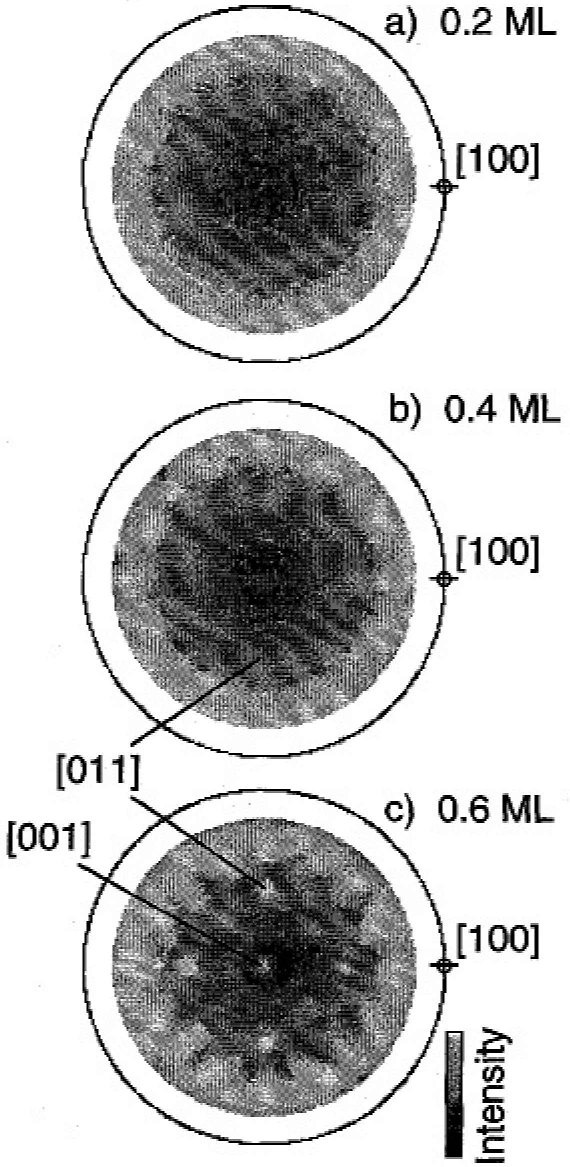

Fig. 4. Au 4d (1405 eV) emission patterns from submonolayer Au/Cu(001) surfaces (Ref. [45]). Low-index crystal directions of prominent forward focusing maxima are indicated.

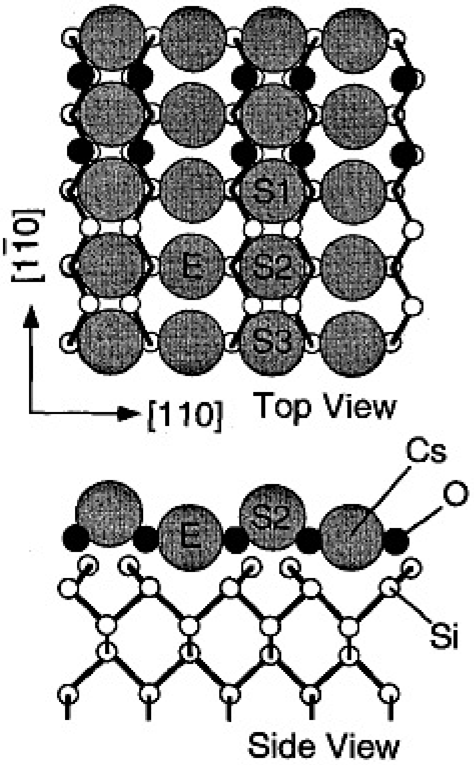

Fig. 5. Illustration of the structure model for the (2×1) Cs/Si(001)–O NEA surface (Ref. [48]).

face obtained by controlled oxidation of a well ordered (2×1) Cs/Si(001) surface. In this study, a wide terrace single-domain (2×1) Si(001) surface was used to prepare a single-domain (2×1) Cs/Si(001) surface. The analysis of the Cs 3d XPD pattern ($E_{kin} = 765$ eV) and comparison with SSC calculations favoured a double layer (DL) model involving two inequivalent positions of Cs atoms above the Si dimer rows. The model is depicted in Fig. 5, specifically in the lower part of the top view, i.e. with no oxygen atoms present. Upon oxidation of this surface up to the work function minimum, which is near 0.5 langmuir exposure, the O 1s and Cs 3d patterns were measured. They find no significant change in the Cs 3d emission pattern upon oxidation, suggesting that the Cs DL structure remains essentially preserved and that oxygen atoms must have penetrated below the Cs double layer. Otherwise new forward focusing maxima due to Cs–O scattering should appear.

The original data of Abukawa et al. [48] are given in Figs. 6a and 7a as linear grey scale plots in the stereographic projection. The experimental Cs 3d pattern of Fig. 6a reflects nicely the local environment

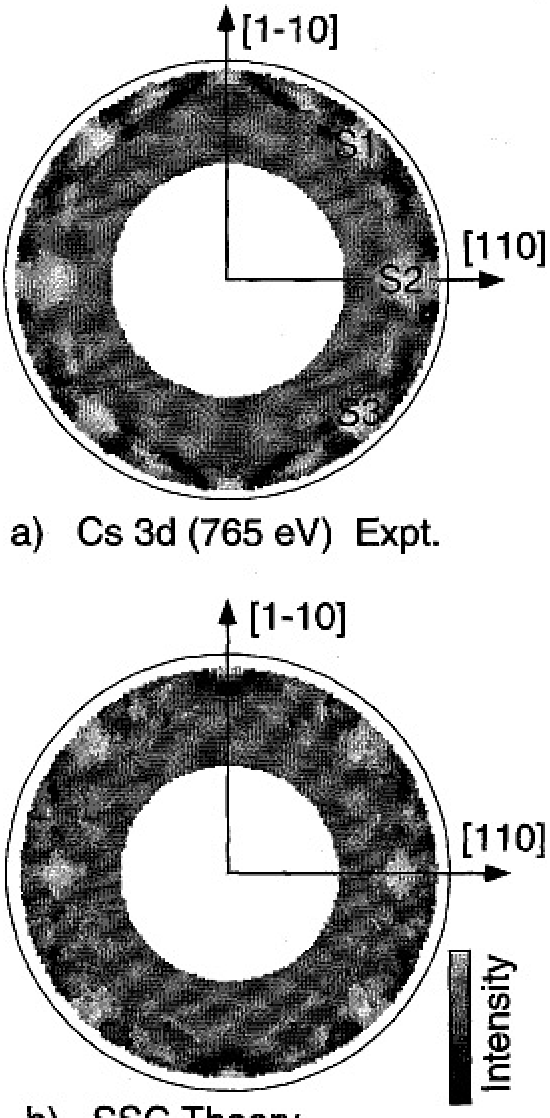

Fig. 6. Stereographic projection of the Cs 3d emission pattern from the (2×1) Cs/Si(001)–O NEA surface. (a) The experimental data are identical to the ones presented in Ref. [48] and have been projected stereographically for the purposes of the present paper. (b) The SSC calculation for the same pattern, also taken from Ref. [48].

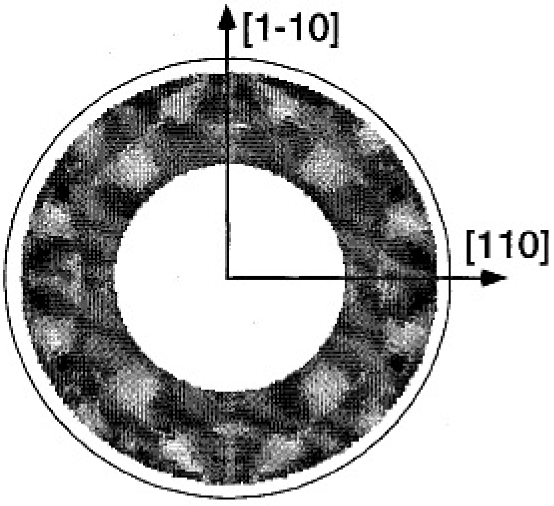

a) O 1s (955 eV) Expt.

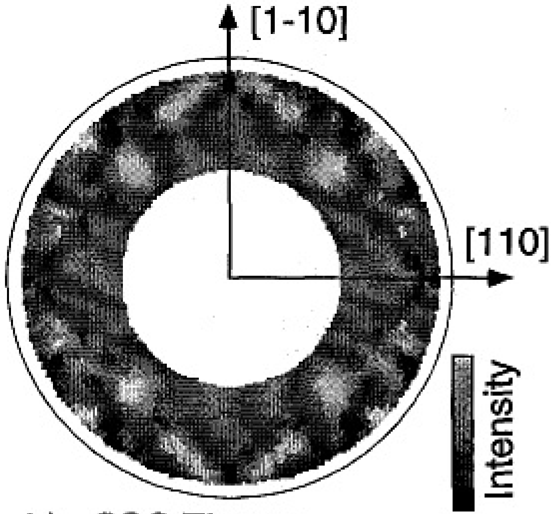

b) SSC Theory

Fig. 7. Same as Fig. 6, but for O 1s emission from the (2×1) Cs/Si(001)–O NEA surface.

of the lower Cs site in the DL structure. The Cs NN atom along the [110] direction (S2, Fig. 5) produces the forward focusing maximum at a polar angle of 76° while the NNN atoms (S1 and S3) produce well defined maxima at slightly higher polar angles near 45° in azimuth. The forward focusing maximum along the [1–10] direction, i.e. along the Cs chains, is just barely outside the solid angle range measured, but the intensity rise towards the maximum is clearly visible at grazing emission. Interestingly this maximum appears to be rather more narrow. This is a well known consequence of multiple forward scattering along atomic chains [36].

The O 1s emission pattern at 955 eV kinetic energy is given in Fig. 7a. Distinct maxima are here observed at polar angles of 65° off normal and 49° away azimuthally from the [110] direction. Obviously these low polar angles, or high takeoff angles, must be produced by O–Cs forward focusing. Knowing from the Cs 3d pattern that the Cs double layer is preserved it is straightforward to find a model with oxygen positions producing these maxima and which is furthermore consistent with the (2×1) translational symmetry. The resulting structure model for the NEA surface is shown in Fig. 5.

Even though this model has been derived essentially from forward focusing peak positions, it is useful to further refine it by means of model calculations. Figs. 6b and 7b show that SSC calculations serve this purpose rather well. Even though the general appearance of the calculated pattern is somewhat more fuzzy, which may be due to the specific scattering approximation used [48], all features of the experiment are well reproduced. In explaining both emission patterns equally well, this XPD structure determination leaves no ambiguities about this structure. As a result from the refinement a vertical separation between oxygen atoms and the lower Cs layer of 0.0 ± 0.1 Å has been found and a lateral separation of oxygen from the axis of the lower Cs chain of 2.2 ± 0.05 Å [48].

5. Surface species

A common feature to XPD/AED patterns from surface species is the absence of forward focusing maxima at non-grazing angles. In this Section we show that there are nevertheless distinctive interference patterns that may be used for a direct identification of the local bonding geometry, and eventually, by means of SSC calculations and *R*-factor analyses, for structure refinement. In Fig. 8 we give adsorbate emission patterns for three different examples of $c(2 \times 2)$ metal-on-metal adsorbate structures on square lattice surfaces: 0.5 ML Au/W(001) [49], 0.25 ML Au/Cu(001) [42], and 0.5 ML Na/Al(001) [50]. In each case an adsorbate core level or Auger line at an energy of the order of 1 keV was measured, which is far in the forward focusing regime. All these data show a fair amount of structure for polar angles higher than 75° and no obvious forward focusing maxima. For the cases of Au/W(001) and Au/Cu(001) it has been verified that the angular distribution at lower polar angles is structureless, and only a ring of more grazing angles has been measured with high accuracy. The full 2π distribution has been measured for Na/Al(001). Care has been taken in all three cases to cover the very grazing angles up to 86–88°.

We shall now illustrate for the case of Au/Cu(001) how the adsorbate structure can be solved to high accuracy by comparison with SSC calculations. It was necessary to measure the emission pattern at a rather low Au coverage, i.e. where the c(2 × 2) LEED superstructure just barely sets in. At slightly higher coverages the appearance of forward focusing maxima due to intermixing completely dominates the much weaker interference pattern of the surface Au species [42]. We have carried out SSC calculations for Au atoms placed in substitutional sites within the surface Cu layer. In Fig. 9 we show how the interference pattern depends on the bonding distance of the Au atoms from the surface, defined by the centers of the Cu atoms. At a vertical Au position of +0.06 Å, which is essentially coplanar with the Cu plane, one clearly finds 8 bright intensity maxima, equally spaced at 45° on the rim of the stereographically projected hemisphere. The ones along the ⟨110⟩ directions are somewhat stronger than the ones along the ⟨100⟩ directions. These maxima can easily be identified as the forward focusing maxima along NN Cu atoms (⟨110⟩) and NNN Au atoms (⟨100⟩, see Fig. 8d). As the adsorption height is varied, the ⟨110⟩ maxima move consistently in angle with the Au–Cu bond angle. At the same time the ⟨100⟩ maxima remain unchanged in shape. The apparent change in brightness is simply due to the grey scale normalization which is carried

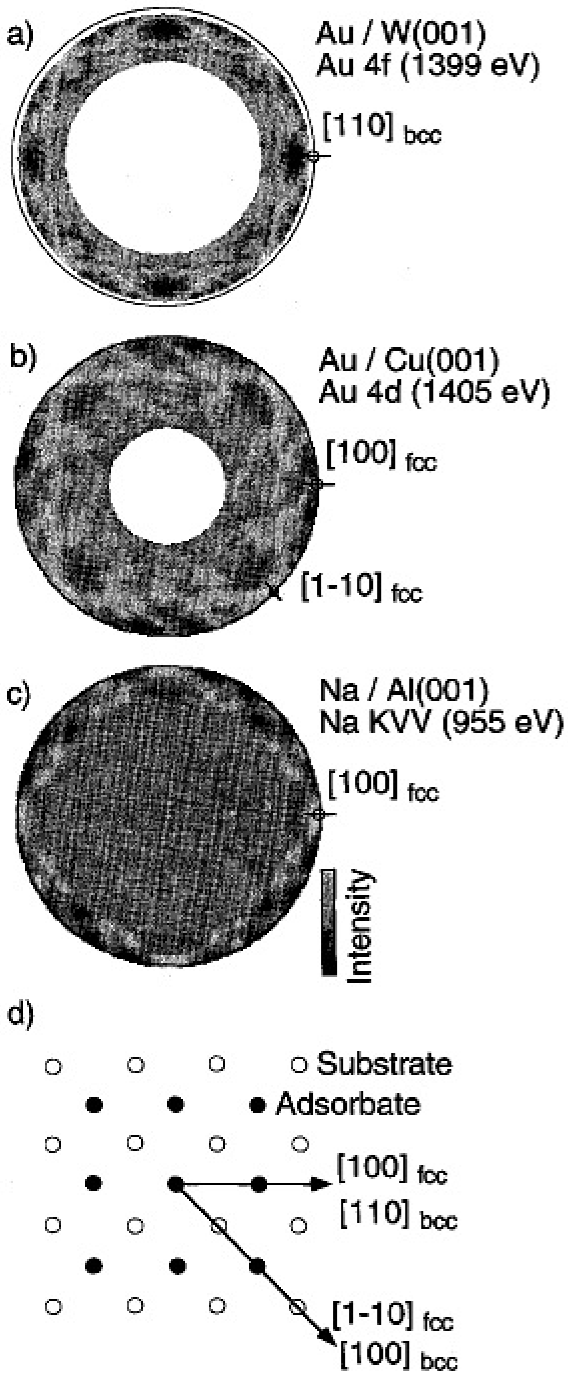

Fig. 8. Adsorbate emission patterns from c(2×2) metal-on-metal structures: (a) Au4f from 0.5 ML Au/W(001) (Ref. [49]), (b) Au4d from 0.25 ML Au/Cu(001) (Ref. [42]), and (c) Na KVV Auger emission from 0.5 ML Na/Al(001) (Ref. [50]). In (d) a schematic top view of these structures is given with principal low-index directions for fcc and bcc substrates indicated.

out individually for each data set. The interference structures in between these maxima change significantly with bond distance, providing therefore an independent means for structure search. In several cases, rings of reduced and enhanced intensity are found concentric with in-plane forward focusing maxima. This tells us that the single scattering processes associated with a particular forward focusing atom dominate the anisotropy inside a cone with a half angle of the order of 20–30°, leading to nearly-axial symmetry inside this cone. On such a ring the phase difference between the non-scattered wave and the wave singly scattered by that atom is 2π, i.e. we have first-order constructive interference (Fig. 1c).

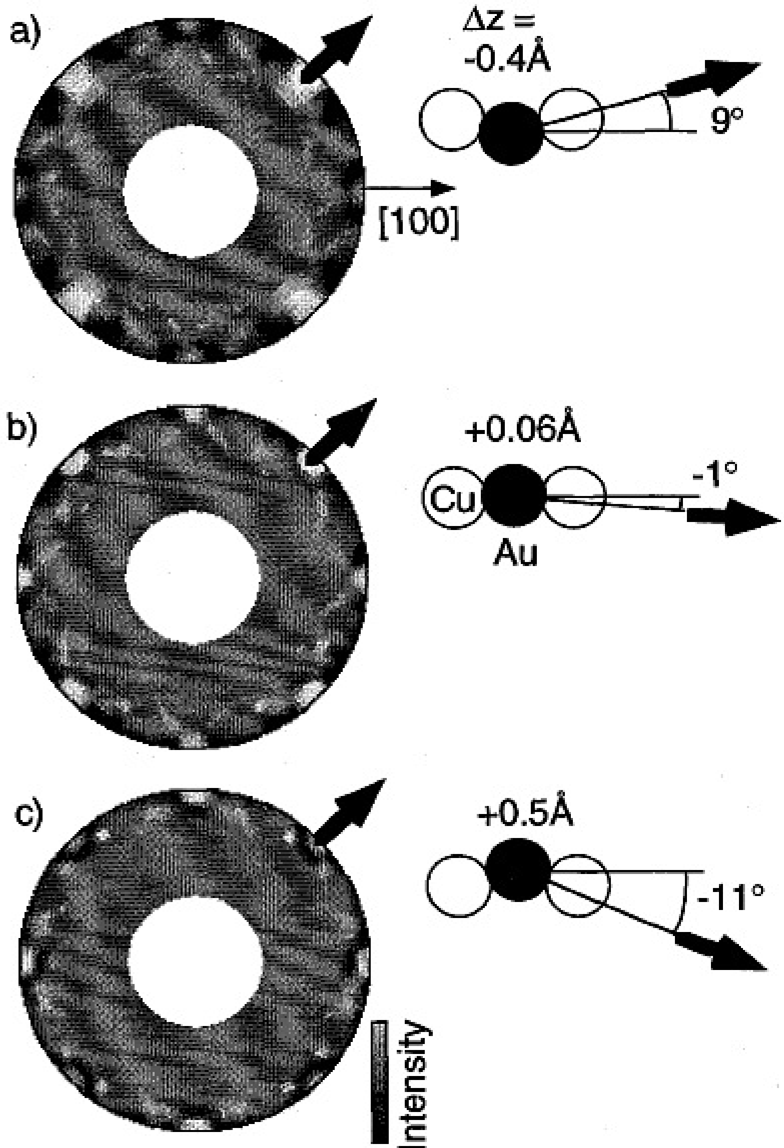

Fig. 9. Au 4d emission patterns (1405 eV) calculated within the SSC approximation for substitutional site occupation of Au in c(2 × 2) 0.25 ML Au/Cu(001). Different vertical spacings Δz of the Au layer relative to the surface Cu layer have been considered as is indicated on the right hand side of each plot.

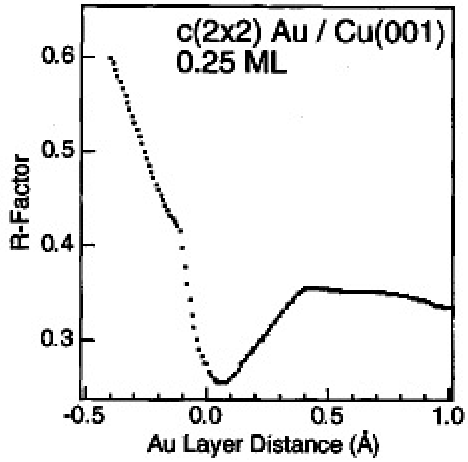

Fig. 10. R-factor curve for the data of Fig. 8b and various vertical Au layer spacings Δz for substitutional sites (see also Fig. 9). A novel R-factor based on multipole expansion coefficients for the full data set [50] has been used.

Fasel et al. [51] have shown that measuring the radii of such interference fringes can provide reasonable bond length values along a particular forward focusing direction, provided that the scattering phase shift is known from theory.

We have carried out an R-factor analysis for the Au/Cu(001) system, for substitutional site occupation with adsorbate distances ranging from -0.4 Å to $+1.0$ Å above the Cu plane. A new type of R-factor has been used which is based on a multipole expansion of the complete data set [12,50]. The result is given in Fig. 10. A very pronounced minimum is found for a vertical distance of 0.06 Å, i.e. Au is essentially coplanar with a very slight outward buckling. This value compares well with the 0.1 Å obtained from a quantitative LEED analysis by Wang et al. [46]. This indicates that single scattering events are dominant enough in such adsorbate emission patterns to permit a meaningful analysis within the SSC approximation. Inspection of the calculated pattern at the R-factor minimum (Fig. 9b) and comparison with the experimental pattern of Fig. 8b shows that the agreement is not perfect, but the positions of the in-plane forward focusing maxima and of dominant interference structures are well reproduced, which seems sufficient to produce this pronounced R-factor minimum.

It is interesting to discuss the character of the R-factor curve. For bonding distances above $+0.4$ Å the variations are relatively small. Here, the Au layer is sufficiently high above the Cu plane to produce an adsorbate diffraction pattern which is essentially representative of the $c(2\times2)$ Au layer alone with little contribution of back-scattering from the substrate. One such pattern is that for $+0.5$ Å given in Fig. 9c. Here, the maximum along $\langle 110\rangle$ in grazing emission is no longer due to Au–Cu NN scattering but due to Au–Au NNN scattering (Fig. 8d). For nearly coplanar geometries, the R-factor appears to be really sensitive to the overall interference structure, including that due to the substrate, while for Au atoms buried deeper below the Cu plane, it is largely dominated by Au–Cu NN forward scattering, i.e. by contributions from a more limited solid-angle range.

We can now verify whether this detailed analysis on one system can sharpen up our eyes for the interpretation of the data from other adsorbate systems, e.g. those shown in Figs. 8a and 8c. For Au/W(001) Takahashi et al. [49] have carried out a similar detailed study, considering both substitutional and overlayer models. Their conclusion was again that SSC calculations do not quantitatively describe the experimental data but nevertheless permit to clearly favour one model over the other. The measured pattern is most consistent with a substitutional adsorbate site very nearly coplanar with the surface tungsten plane. The structure is thus very similar to what we found for Au/Cu(001). The two patterns of Figs. 8a and 8b show indeed some similarities in their interference structures, most prominently the characteristic bright rounded square with corners at the NN forward focusing directions. It is noteworthy that the calculated patterns for the two structures (Fig. 3b of Ref. [49] and Fig. 9b of this work) are even closer to each other, indicating that the differences of the two substrate materials W(001) and Cu(001) reflect themselves more strongly in phenomena that are beyond the SSC description. These might be multiple scattering effects, which are expected to be stronger in tungsten due to the stronger scattering potential.

Compared to the two Au adsorbate patterns (Figs. 8a and 8b), the Na KVV pattern from $c(2\times2)$ Na/Al(001) shows more distinct differences. The rounded square structure is missing, and the Na–Al

NN forward focusing maxima along ⟨110⟩ are much weaker than the Na–Na maxima along ⟨100⟩. There is some similarity of the overall pattern with that of Fig. 9c. This tells us immediately that the adsorbate position is here considerably above the substrate surface plane. A distance of 1.22 Å has been found by Fasel et al. [50] from an extensive *R*-factor analysis of the Na 1s emission pattern at a very low energy of 182 eV, where much more interference structure is present.

6. Conclusions

The routine measurement of 2π-scans has brought an immense progress to the application of XPD and AED for surface structure determination. This is not simply due to an increase of the data base, but the representation of such patterns in a LEED-screen type fashion (actually the projection is here stereographic) adds the important factor of intuition, because the human eye can now easily recognize common features in different patterns. We have shown that such common features exist in patterns from subsurface *and* surface species, independent of the type of atoms involved in the photoemission or scattering processes. They may serve as fingerprints of the local surface geometry. For surface and near-surface species a meaningful structure refinement can be carried out by means of *R*-factor analyses using SSC calculations. The combination of this accurate method with the intuition obtained from fingerprints renders such structure determinations very reliable.

Acknowledgements

We are indebted to O. Raetzo, E. Mooser, H. Tschopp and F. Bourqui for excellent technical support. This work has been supported by the Swiss National Foundation.

References

[1] C.S. Fadley, in: Progress in Surface Science, Vol. 16, Ed. S.G. Davison (Pergamon, New York, 1984) p. 275.
[2] W.F. Egelhoff, Jr., Crit. Rev. Solid State Mater. Sci. 16 (1990) 213.
[3] J. Osterwalder, Arab. J. Sci. Technol. 15 (1990) 273.
[4] S.A. Chambers, Adv. Phys. 40 (1991) 357.
[5] C.S. Fadley, in: Synchrotron Radiation Research: Advances in Surface Science, Ed. R.Z. Bachrach (Plenum, New York, 1990) ch. 11.
[6] S.A. Chambers, Surf. Sci. Rep. 16 (1992) 261.
[7] H.P. Bonzel, Prog. Surf. Sci. 42 (1993) 219.
[8] C.S. Fadley, Surf. Sci. Rep. 19 (1993) 231.
[9] A. Szöke, in: Short Wavelength Coherent Radiation: Generation and Applications, Eds. D.T. Attwood and J. Boker, AIP Conf. Proc. No. 147 (AIP, New York, 1986).
[10] J.J. Barton, Phys. Rev. Lett. 61 (1988) 1356.
[11] S.Y. Tong, H. Huang and Hua Li, in: Advances in Surface and Thin Film Diffraction, Eds. T.C. Huang, P.I. Cohen and D.J. Eaglesham, MRS Symp. Proc. No. 208 (MRS, Pittsburgh, 1991) p. 13.
[12] J. Osterwalder, R. Fasel, A. Stuck, P. Aebi and L. Schlapbach, J. Electron Spectrosc. Relat. Phenom. 68 (1994) 1.
[13] M. Zharnikov, D. Mehl, M. Weinelt, P. Zebisch and H.-P. Steinrück, Surf. Sci. 306 (1994) 125.
[14] L.-G. Petersson, S. Kono, N.F.T. Hall, C.S. Fadley and J.B. Pendry, Phys. Rev. Lett. 42 (1979) 1545.
[15] W.F. Egelhoff, Jr., Phys. Rev. B 30 (1984) 1052.
[16] H.C. Poon and S.Y. Tong, Phys. Rev. B 30 (1984) 6211.
[17] D. Naumovic, A. Stuck, T. Greber, J. Osterwalder and L. Schlapbach, Phys. Rev. B 47 (1993) 7462.
[18] R.J. Baird, C.S. Fadley and L.F. Wagner, Phys. Rev. B 15 (1977) 666.
[19] H. Li and B.P. Tonner, Phys. Rev. B 37 (1988) 3959.
[20] M. Seelmann-Eggebert and H.J. Richter, J. Vac. Sci. Technol. B 9 (1991) 1861.
[21] J. Osterwalder, T. Greber, A. Stuck and L. Schlapbach, Phys. Rev. B 44 (1991) 13764.
[22] D.G. Frank, T. Golden, O.M.R. Chyan and A.T. Hubbard, J. Vac. Sci. Technol. A 9 (1991) 158.
[23] H.A. Engelhardt, W. Bäck, D. Menzel and H. Liebl, Rev. Sci. Instrum. 52 (1981) 835.
[24] R.C.G. Leckey and J.D. Riley, Appl. Surf. Sci. 22/23 (1985) 196.
[25] S. Kono, N. Nakamura, K. Anno and S. Teruyama, Surf. Sci. 271 (1992) 596.
[26] D.E. Eastman, J.J. Donelon, C. Hien and F.J. Himpsel, Nucl. Instrum. Methods (1980) 327; D. Rieger, R.D. Schnell, W. Steinmann and V. Saile, Nucl. Instrum. Methods 208 (1983) 777.
[27] H. Daimon and S. Ino, Rev. Sci. Instrum. 61 (1990) 57.
[28] L.J. Terminello, J.J. Barton and D.A. Lapiano-Smith, Phys. Rev. Lett. 70 (1993) 599.
[29] B. Eisenhut, J. Stober, G. Rangelov and Th. Fauster, Phys. Rev. B 47 (1993) 12980; B. Eisenhut, J. Stober, G. Rangelov and Th. Fauster, Phys. Rev. B 49 (1994) 14676.
[30] A.P. Kaduwela, D.J. Friedman and C.S. Fadley, J. Electron Spectrosc. Relat. Phenom. 57 (1991) 223.
[31] V. Fritzsche, J. Phys. Condensed Matter 2 (1990) 1413.
[32] R. Gunnella, C.R. Natoli, Z.Y. Wu and M. Pallotta, to be published.

[33] C.H. Li, A.R. Lubinsky and S.Y. Tong, Phys. Rev. B 17 (1978) 3128.
[34] S.Y. Tong, H.C. Poon and D.R. Snider, Phys. Rev. B 32 (1985) 2096.
[35] M.-L. Xu, J.J. Barton and M.A. Van Hove, Phys. Rev. B 39 (1989) 8275.
[36] H.A. Aebischer, T. Greber, J. Osterwalder, A.P. Kaduwela, D.J. Friedman, G.S. Herman and C.S. Fadley, Surf. Sci. 239 (1990) 261.
[37] Y.U. Idzerda and D.E. Ramaker, Phys. Rev. Lett. 69 (1992) 1943.
[38] T. Greber, J. Osterwalder, D. Naumovic, A. Stuck, S. Hüfner and L. Schlapbach, Phys. Rev. Lett. 69 (1992) 1947.
[39] D.E. Ramaker, H. Yang and Y.U. Idzerda, J. Electron Spectrosc. Relat. Phenom. 68 (1994) 63.
[40] P. Aebi, unpublished.
[41] D. Naumovic, J. Osterwalder, A. Stuck, P. Aebi and L. Schlapbach, Surf. Sci. 287/288 (1993) 950.
[42] D. Naumovic, Doctoral Thesis, Université de Fribourg (1993).
[43] P. Schwaller, P. Aebi, J. Osterwalder, L. Schlapbach, M. Shimoda, T. Mochiku and K. Kadowaki, Phys. Rev. B 48 (1993) 6732.
[44] Y.S. Luo, Y.-N. Yang and J.H. Weaver, Phys. Rev. B 46 (1992) 1114.
[45] D. Naumovic, A. Stuck, T. Greber, J. Osterwalder and L. Schlapbach, Surf. Sci. 269/270 (1992) 719; 277 (1992) 235.
[46] Z.Q. Wang, Y.S. Li, C.K.C. Lok, J. Quinn, F. Jona and P.M. Marcus, Solid State Commun. 62 (1987) 181.
[47] D.D. Chambliss and S. Chiang, Surf. Sci. 264 (1992) L187.
[48] T. Abukawa, S. Kono and T. Sakamoto, Jpn. J. Appl. Phys. 28 (1989) L303.
[49] H. Takahashi, M. Sasaki, S. Suzuki, S. Sato, T. Abukawa, S. Kono and J. Osterwalder, Surf. Sci. 304 (1994) 65.
[50] R. Fasel, P. Aebi, J. Osterwalder, L. Schlapbach, R.G. Agostino and G. Chiarello, Phys. Rev. B 50 (1994) 14516.
[51] R. Fasel, P. Aebi, J. Osterwalder and L. Schlapbach, Surf. Sci. 331–333 (1995) 80.